ЖУРНАЛ СТРУКТУРНОЙ ХИМИИ

2013. Том 54, № 2 *Март – апрель* *С. 220 – 227*

UDC 541.6:547.13:546.65

COMPUTATIONAL STUDY ON THE STRUCTURE AND PROPERTIES OF TERNARY COMPLEXES OF Ln^{3+} (Ln = La, Ce, Nd AND Sm) WITH 5,7-DICHLOROQUINOLINE-8-OL AND 4-VINYL PYRIDINE

T. Hosseinnejad[1], S.J. Ahmadi[2], M.H. Karimi-Jafari[3]

[1]*Department of Chemistry, Faculty of Science, Alzahra University, Vanak, Tehran, Iran*
E-mail: tayebeh.hosseinnejad@gmail.com
[2]*Nuclear Science and Technology Research Institute (NSTRI), Tehran, Iran*
[3]*Institute of Biochemistry and Biophysics, University of Tehran, Tehran, Iran*

Received November, 13, 2011 *Revised — January, 14, 2012*

In the present research, we have mainly concentrated on the survey of interactions in Ln^{3+} (Ln = La, Ce, Nd and Sm) ternary complexes of 5,7-dichloroquinoline-8-ol (DCQ) and 4-vinyl pyridine (VP), $[Ln(VP)_2(DCQ)_3]^{3+}$ by means of density functional theory, Hartree-Fock and Sparkle/PM3 semi-empirical computational methods. For VP and DCQ ligands, the cation binding energy sequence follows the order $La^{3+} > Ce^{3+} > Nd^{3+} > Sm^{3+}$ as expected based on increasing in the hardness and decreasing in the ionic radius of this lanthanide cation series. A similar trend was observed in the calculated binding energy of the aforesaid ligands with the hydrated lanthanide cation series $[Ln(H_2O)_9]^{3+}$, while the computed values of deformation energy of ligands upon complexation demonstrated an opposite order in the lanthanide cation series. Moreover, the solvent effects are considered via a polarized continuum model and provided a significant increase in the binding strength while the relative magnitude of binding energies is the same as that in the gas phase. Combining quantum and statistical mechanical calculations, we have also determined quantitatively a reliable estimate of the conformational distribution of the $[Sm(VP)_2(DCQ)_3]^{3+}$ complex at various temperatures in the gas phase by computing the molecular partition functions and consequently the analysis of the conformational equilibrium constants.

K e y w o r d s: ion imprinting, lanthanide complexes, density functional theory, polarized continuum model, conformational distribution.

INTRODUCTION

In contrast with a large amount of theoretical studies on alkali and earth alkali cations, transition metals and metalloids, computational reports dealing with actinides and lanthanides are rather scarce. In the present work, we have provided a computational study on Ln^{3+} (Ln = La, Ce, Nd and Sm) ternary complexes of 5,7-dichloroquinoline-8-ol and 4-vinyl pyridine (hereafter denoted by DCQ and VP respectively; Fig. 1) to assess the intrinsic interaction energies and structural features of the complexes. The main motivation of our study on this system was the technological and fundamental importance of the ternary complexes of metal cations with DCQ and VP functional monomers that recently have been synthesized for selective separation of some metal cations on the basis of ionic imprinting process [1—6].

Molecular imprinting is a versatile technique for preparing polymeric SPE (solid phase extraction) adsorbents capable of high molecular recognition. This method involves the arrangement of functional monomers around a template molecule. Subsequent polymerization results in trapping the tem-

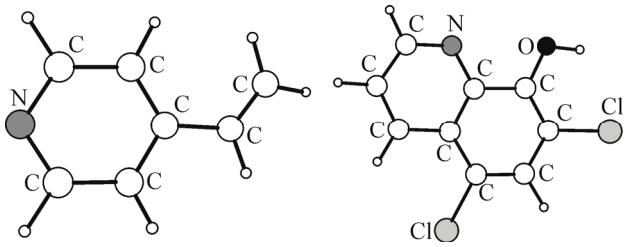

Fig. 1. Schematic representation of ligands: 4-vinyl pyridine (VP) and 5,7dichloroquinoline-8-ol (DCQ)

plate in a highly cross-linked polymer matrix. Extraction of the imprint molecules from the matrix leaves a predetermined arrangement of ligands and tailored binding pockets that are complementary in size and shape to the analyte molecule or ion. Prasada Rao *et al*. [7, 8] have reviewed on the topic entitled ″Tailored ion-imprinted polymer materials for solid phase extraction of inorganics″. They discussed various factors that determine the formation and recognition properties of binding sites of ion imprinted polymers (IIPs), such as the template size and shape, the binding strength of interaction sites and functional monomer-template rigidity.

It should be noticed that there are many reports on the lanthanide ion imprinted polymer preparation [4—6]especially during the past years, which describe a preconcentrative separation of lanthanide cations by co-polymerizing $[Ln(VP)_2(DCQ)_3]^{3+}$ ternary complexes, styrene and a cross linker, e.g. divinyl benzene, in the presence of 2,2′-azo bis isobutylonitrile as an initiator. Since the first step in the imprinting is the pre-arrangement of the template and functional monomers in a solvent, the theoretical knowledge of interactions and structural properties of pre-polymerization complexes affects strongly the affinity and selectivity of synthesized IIPs.

In the present investigation, we shall concentrate on the quantum chemistry calculation of intrinsic interactions of lanthanide cations Ln^{3+} with DCQ and VP ligands from the structural and energetic viewpoints. Our aim was first to assess the gas phase binding energies of VP and DCQ ligands with Ln^{3+} cations with respect to the optimized geometry of $[Ln(VP)_2(DCQ)_3]^{3+}$ complexes. Trends of metal—ligand bond distances were also discussed and compared with the trend of the ionic radius within the series of lanthanide cations. Additionally, we have analyzed the binding energies of the aforesaid ligands with the hydrated lanthanide cations $[Ln(H_2O)_9]^{3+}$ in comparison with the non-hydrated lanthanide cations.

In addition to ion—ligand interactions, solvation plays an important role in the ion imprinting process. Furthermore, because of the strong electrostatic character of the metal—ligand interactions, which remains effective beyond the first and even second coordination sphere, structural parameters are sensitive to the solvent effect. So, we have also estimated solvent effects on the structure and binding energies of ligands in $[Ln(VP)_2(DCQ)_3]^{3+}$ complexes by concerning a continuum representation of the solvent surrounding the complexes via the polarized continuum model [9—11] (PCM), which led to a significant decrease in the computed binding energies. We have also determined the deformation energies of ligands upon complexation that allow us to judge the size and hardness effect of lanthanide cations on the structural changes of the geometrically relaxed ligands.

Another objective of this work is quantifying and analyzing the conformational distribution of various structures of the $[Sm(VP)_2(DCQ)_3]^{3+}$ ternary complex over local minima of the potential energy hyper-surface. It should be stated that imprinted polymer of the samarium cation has recently been synthesized by Ahmadi and coworkers on the basis of the pre-polymerization $[Sm(VP)_2(DCQ)_3]^{3+}$ ternary complex [4].

In this respect, we have employed the standard statistical mechanical formalisms [12] for the determination of electronic, rotational, and vibrational contributions to the partition function and hence, conformational equilibrium constants at various temperatures based on the results of density functional theory (DFT). Then, a population analysis has been performed on the obtained values of conformational concentrations to investigate the effect of internal degrees of freedom on the stability of conformers of the $[Sm(VP)_2(DCQ)_3]^{3+}$ complex in the 298.15—498.15 K temperature range.

COMPUTATIONAL METHODS

All $[Ln(VP)_2(DCQ)_3]^{3+}$ complexes and non-coordinated VP and DCQ ligands were fully optimized by quantum mechanical calculations at HF and DFT levels of theory. All DFT calculations reported here have been performed using the nonlocal hybrid Becke's three-parameter exchange functional denoted as B3LYP [13]. It should be stated that some previous studies claim that the HF level of theory (in comparison with DFT and MP2 calculations) is sufficient for the reasonable description of the structural and energetic features of lanthanide complexes [14]. In the present work, this issue is investigated more thoroughly through a comparison of the obtained results of HF and DFT optimizations. The harmonic frequencies have been calculated to ensure that the obtained optimized structures of complexes are true minima.

It is noteworthy that the initial conformations of all $[Ln(VP)_2(DCQ)_3]^{3+}$ complexes in the geometry optimization process were deduced by carrying out a conformational search procedure based on the sparkle/PM3 semi-empirical method [15—19]. In all these calculations the eigenvector following (EF) routine for searching minima was used as an optimizer, and geometry optimizations were performed in Cartesian coordinates. The convergence criteria for the gradient and SCF procedure were adapted as 0.01 kcal$\cdot$ Å^{-1} mol^{-1} and 10^{-10} kcal$\cdot$mol^{-1} respectively. In the parameterization of the sparkle model for the lanthanide complexes, 4*f* orbitals are contracted towards the ion by the outermost 5*s* and 5*p* closed shells and the lanthanide ion was represented by a sparkle. This sparkle, which has a columbic charge of +3*e*, is superimposed to a repulsive exponential potential of the form $\exp(-\alpha r)$, where α accounts for the size of the lanthanide ion [15].

The choice of the sparkle/PM3 semi-empirical method for the prediction of the initial geometry was motivated by the facts that (*i*) to our knowledge, no X-ray crystallographic structural data have been reported for $[Ln(VP)_2(DCQ)_3]^{3+}$ complexes; (*ii*) sparkle/PM3 is a reliable paradigm to predict the geometry of lanthanide complexes formed by just oxygen and nitrogen donors in the coordination polyhedron [15]; (*iii*) the accuracy of this method is competitive with the *ab initio*/effective core potential calculations especially for the large-size lanthanide complexes, while the former being hundreds of times faster [20—25]. The conformational search involved the geometry optimization of 500 random initial structures for complexes. These initial geometries have been produced randomly by varying the coordination variables which control the relative orientation of surrounding arrays of DCQ and VP ligands around the lanthanide cations.

It is remarkable to note that the application of HF and DFT methods in these systems containing 84 atoms with a rare-earth ion carrying 4*f* electrons would need very large computational times and resources. In order to overcome some of these difficulties, we have applied the quasi-relativistic effective core potentials (RECPs) of Stuttgart group [26, 27] to the lanthanide ions. Accordingly, the 46 core and 4*f* electrons of lanthanide ions are replaced with these RECPs that implicitly take into account relativistic effects. For the valence orbitals the corresponding basis sets associated with the core pseudo-potential were used [27—29]. On the other atoms, the 6-31G***** basis set was employed throughout this investigation [30—32]. All HF and DFT calculations were performed using the GAMESS suite of programs [33], and the MOPAC 2009 package [34] was utilized for semi-empirical calculations.

RESULTS AND DISCUSSION

We first investigated the interaction of the Ln^{3+} cation series with two VP and three DCQ ligands in the gas phase. The energy values of the optimized structure of $[Ln(VP)_2(DCQ)_3]^{3+}$ complexes together with the calculated binding energies of ligands in the aforementioned complexes (ΔE_{bind}) at the HF and DFT levels of theory have been given in Table 1. The binding energy is defined as follows:

$$Ln^{3+} + 2(VP) + 3(DCQ) \xrightarrow{\Delta E_{bind}} [Ln(VP)_2(DCQ)_3]^{3+}. \quad (1)$$

In the optimized geometry of all $[Ln(VP)_2(DCQ)_3]^{3+}$ complexes, two pyridine and three quinoline groups of ligands create a cage-like structure which can work as a cavity with a high potential to support selectivity.

Table 1

Electronic energies of $[Ln(VP)_2(DCQ)_3]^{3+}$ *and* $[Ln(H_2O)_9]^{3+}$ *clusters* (Ln = La, Ce, Nd *and* Sm), *binding energies and the mean optimized* Ln—N *distances from* HF *and* DFT *optimizations*

Ln	Electronic energy of $[Ln(VP)_2(DCQ)_3]^{3+}$, Hartree		Electronic energy of $[Ln(H_2O)_9]^{3+}$, Hartree		ΔE_{bind}, kcal·mol^{-1}		$\Delta E_{bind,aq}$, kcal·mol^{-1}		Mean Ln—N distance, Å	
	HF	DFT	HF	DFT	HF	DFT	HF	DFT	HF	DFT
La	–4853.83	–4871.42	–714.762	–718.717	–518.937	–559.32	–16.08	–12.89	2.73	2.70
Ce	–4854.49	–4872.08	–715.409	–719.367	–528.793	–569.93	–18.58	–15.46	2.71	2.68
Nd	–4855.74	–4834.73	–716.660	–720.623	–544.561	–586.63	–20.61	–17.02	2.67	2.65
Sm	–4856.96	–4874.56	–717.874	–721.842	–558.696	–602.00	–22.15	–18.82	2.64	2.61

The summarized results of binding energies (ΔE_{bind}) in Table 1 indicates that (*i*) among two levels of computation, the B3LYP/631G* level leads to more negative binding energy values in comparison with those obtained at the HF/631G* level, which can be attributed to the inclusion of electron correlation effects in DFT calculations and (*ii*) in the cation series, binding energies at the HF and DFT levels decrease with an increase in the cation hardness by about 50 kcal·mol^{-1} from La^{3+} to Sm^{3+}. Moreover, the average optimized Ln—N distance per ligand has been computed at the HF and DFT levels and listed for the complexes in the last column of Table 1. As can be seen from Table 1, firstly, at the DFT level of theory the mean Ln—N distance is less than those obtained at the HF level and second, in the Ln^{3+} cation series, the mean Ln—N distance ranging from about 2.7 Å to 2.6 Å is shortened by a step size of around 0.03 Å from La^{3+} to Sm^{3+}. This finding in the calculated values of the mean Ln—N distance correlates with two facts: (*i*) the calculated increasing trend in the metal—ligand binding strength of the complexes and (*ii*) diminution of the ionic radius of lanthanide cations tabulated by Shannon [35] and David [36, 37].

It is noteworthy that the agreement between the calculated trends in the mean Ln—N bond length of $[Ln(VP)_2(DCQ)_3]^{3+}$ complexes with the ionic radius of lanthanide cations can be attributed in a large part to the predominant electrostatic nature of the metal—ligand bond in these complexes, which is slightly more pronounced for lanthanides than actinides [38, 39]. In the next step, we have considered the complexation of the trivalent lanthanide aqua cations $[Ln(H_2O)_9]^{3+}$ with the aforesaid ligands. The corresponding reaction is defined as the following:

$$[Ln(H_2O)_9]^{3+} + 2(VP) + 3(DCQ) \xrightarrow{\Delta E_{bind,aq}} [Ln(VP)_2(DCQ)_3]^{3+} + 9H_2O. \quad (2)$$

To this end, the energies of hydrated lanthanide cations were calculated with respect to their optimized structures at the HF and DFT levels of theory. Then, the binding energies of ligands in $[Ln(VP)_2(DCQ)_3]^{3+}$ complexes were determined in the presence of aqua lanthanide cations. This quantity was defined as $\Delta E_{bind,\,aq}$ (in Eq. 2.) and has been reported together with the computed energies of $[Ln(H_2O)_9]^{3+}$ clusters at the HF and DFT levels of theory in Table 1. Analysis of the calculated values of $\Delta E_{bind,\,aq}$ shows that although the order of binding energies of ligands towards $[Ln(H_2O)_9]^{3+}$ follows the same trend as Ln^{3+}, however, it leads to an increase of around 500 kcal·mol^{-1} in the calculated binding energies. Obviously, this additional energy cost is a result of more energetically favored hydrated lanthanide cations (presented in Eq. 2) in comparison with bare lanthanide ions (defined in Eq. 1). It should be noticed that the values of $\Delta E_{bind,\,aq}$ obtained at the HF level are more negative than those calculated at the DFT level. This behavior is contrary to what we have observed in the comparison of ΔE_{bind} values calculated at HF and DFT levels.

As remarked previously, because of the strong ionic nature of lanthanide-ligand interactions in the complexes of interest we expect that the characteristics of lanthanide-ligand bonds are strongly sensitive to the presence of long-range solvent effects. Thus we have considered computationally the complexation reactions of the Ln cation series with the aforesaid ligands in an aqueous solution, which lead to the formation of $[Ln(VP)_2(DCQ)_3]^{3+}$ complexes. In this respect, the geometry optimization of all species was carried out through the polarized continuum model (PCM) at HF and DFT levels.

Table 2

Electronic energies and binding energies of PCM solvated $[Ln(VP)_2(DCQ)_3]^{3+}$ *complexes and the deformation energy of ligands upon complexation* ΔE_{def} (*See text for its concise definition*)

Ln	Electronic energy of solvated complex, Hartree		$\Delta E_{bind,PCM}$, kcal·mol^{-1}		ΔE_{def}, kcal·mol^{-1}	
	HF	DFT	HF	DFT	HF	DFT
La	–4854.23	–4871.81	–735.95	–817.69	25.48	18.04
Ce	–4854.87	–4872.46	–741.25	–825.85	25.53	18.18
Nd	–4856.13	–4873.72	–757.90	–842.78	27.34	19.60
Sm	–4857.35	–4874.94	–772.37	–859.21	29.19	20.62

These calculated PCM results for the electronic energies and binding energies of ligands in $[Ln(VP)_2(DCQ)_3]^{3+}$ complexes have been listed in Table 2.

A comparison of the PCM calculations of binding energies with the gas phase values at HF and DFT levels implies that they still follow the order $La^{3+} > Ce^{3+} > Nd^{3+} > Sm^{3+}$, but the computed values of binding energies decrease considerably (by more than about 200 kcal·mol^{-1}), showing slightly stronger lanthanide-ligand bonds. The results of this comparison have been illustrated in Fig. 2. It is noteworthy that PCM calculations at the B3LYP/631G* level predict stronger bindings in comparison with those obtained at the HF/631G* level, as already discussed for the calculated binding energies in the gas phase.

Upon complexation of ligands with lanthanide cations, significant changes in the geometric and energetic character of free ligands occur, which can be described quantitatively by a calculation of the deformation energy (denoted by ΔE_{def}). Thus, we have determined the deformation energy of the ligands as the energy difference between the structures of free ligands and ligands within the complexes at HF and DFT levels of theory and tabulated them in the last column of Table 2. As expected, the order of the calculated deformation energies with respect to the lanthanide cation series leads to the sequence $La^{3+} < Ce^{3+} < Nd^{3+} < Sm^{3+}$ at HF and DFT levels of theory and consequently, indicates that the ligands are more deformed with harder metals. Furthermore, the result presented in Table 2 shows that the deformation energies calculated at the DFT level are less than those obtained by HF calculations. In Fig. 3, we have made a comparison between the trend of HF and DFT calculated deformation energies with the corresponding binding energies in the $[Ln(VP)_2(DCQ)_3]^{3+}$ complexes. As it has been displayed in Fig. 3, the trend described above for the deformation energy was observed in the reverse order for the biding energy of $[Ln(VP)_2(DCQ)_3]^{3+}$ complexes.

In the next stage, we focused our attention on the conformational distribution of the $[Sm(VP)_2(DCQ)_3]^{3+}$ complex by determining the equilibrium constants of conversion reactions be-

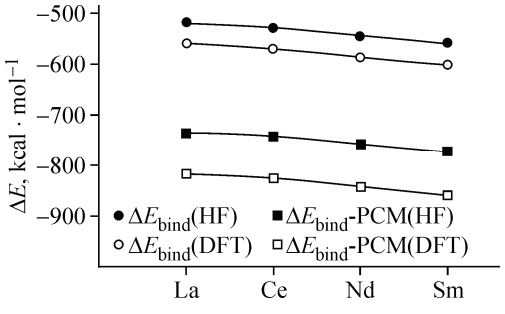

Fig. 2. Binding energies in the gas phase (ΔE_{bind}) and binding energies by the PCM solvent effect model ($\Delta E_{bind, PCM}$) calculated at HF and DFT levels of theory in $[Ln(VP)_2(DCQ)_3]^{3+}$ complexes with Ln = La, Ce, Nd and Sm

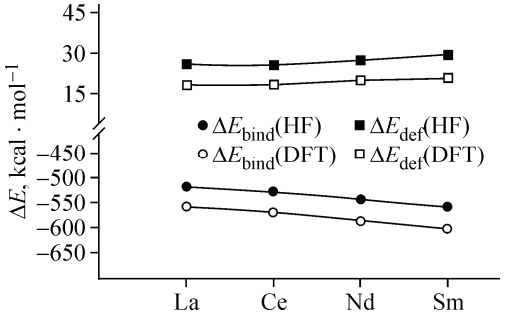

Fig. 3. Binding energies (ΔE_{bind}) and deformation energies (ΔE_{def}) calculated at HF and DFT levels of theory in $[Ln(VP)_2(DCQ)_3]^{3+}$ complexes with Ln = = La, Ce, Nd and Sm

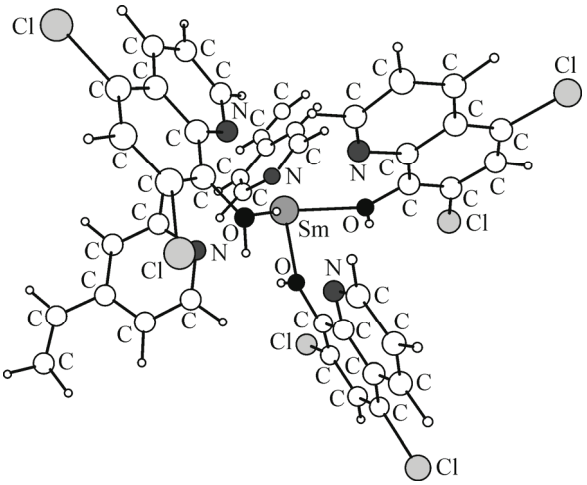

Fig. 4. Optimized structure of the most stable conformer of the $[Sm(VP)_2(DCQ)_3]^{3+}$ complex (C_{ref})

tween the most stable conformers. In order to produce a reasonable set of the most stable conformers, the following procedure was performed. First, the aforementioned results of sparkle/PM3 optimizations were analyzed and followed by further optimizations at the B3LYP/631G* level of theory. Finally, among the produced structures, five of them were selected that cover a conformational energy range of around 1 kcal·mol^{-1} higher than the electronic energy of the global minimum. In Fig. 4, based on the electronic energy values obtained from DFT geometry optimization calculations, we have illustrated the structure of the most stable conformer of the $[Sm(VP)_2(DCQ)_3]^{3+}$ complex. For these 5 conformers, the moments of inertia, vibrational frequencies and ground-state electronic and zero-point energies were calculated at the DFT level of theory in order to present a population analysis at various temperatures according to the following statistical mechanical approach [12].

In this manner, the structure with the lowest value of the electronic energy was selected as the reference conformer (expressed as C_{ref}) and the conformational conversion reaction was defined as the following:

$$C_I \rightarrow C_{ref}, \tag{3}$$

where C_I denotes any of the other conformers. The equilibrium constant of this conversion reaction can be related to the values of the molecular partition function as the following:

$$K_{I,ref} = \frac{q_{ref}}{q_I}. \tag{4}$$

Based on the factorization property of the partition function, the equilibrium constant $K_{I,ref}$ is generally considered as the product of electronic (K_{elec}), rotational (K_{rot}), and vibrational (K_{vib}) contributions and is given by

$$K_{I,ref} = K_{elec} K_{rot} K_{vib} = \frac{q_{elec,ref}}{q_{elec,I}} \frac{q_{rot,ref}}{q_{rot,I}} \frac{q_{vib,ref}}{q_{vib,I}}, \tag{5}$$

where q_{elec}, q_{rot}, and q_{vib} are the electronic, rotational, and vibrational parts of the partition function respectively, which can be determined from the standard formalism of the equilibrium statistical mechanics [12, 40]. It should be stated that this factorization adopted in Eq. (5) makes it possible to analyze in a distinct manner the role of the electronic, rotational, and vibrational degrees of freedom on the relative population of each conformer.

In Table 3 we have reported the molecular partition function ratios for the electronic, vibrational, and rotational contributions of the most stable conformer (expressed as C_{ref}) and those corresponding to the other conformers at 298.15 K. The product of these ratios ($K_{I,ref}$ listed in Table 3) yields the concentration of the most stable conformer (C_{ref}) relative to that of the Ith conformer (C_I). The calculated relative electronic energies of all conformers, their electronic contribution to the conformational distribution and total conformational distribution percents have also been presented in Table 3. It is important to mention that for all conformers, the zero-point energy correction has been considered in the calculation of the electronic contribution to the conformational distribution percents. In this Table, all conformations were ordered according to the increase in relative electronic energies.

As it can be seen from both electronic conformational distribution values and total conformational distribution percents, the presence of the conformer C_{ref} in the gas phase is favored with respect to all the other conformers. The results presented in Table 3 indicate that the calculated values of K_{rot} are around unity in all conformers and hence, none of them has a considerable preference over the other

Table 3

Relative electronic energies ($E_{elec,relative}$), *electronic*, *vibrational and rotational contribution of conformational equilibrium constants* (K_{elec}, K_{vib} *and* K_{rot}), *total conformational equilibrium constants* ($K_{I,ref}$), *electronic contribution of conformational distribution percents, and total conformational distribution percents for* $[Sm(VP)_2(DCQ)_3]^{3+}$ *complex*

Conformer	$E_{elec,relative}$, kcal·mol^{-1}	K_{elec}	K_{vib}	K_{rot}	$K_{I,ref}$	$G_{relative}$, kcal·mol^{-1}	Electronic conformational distribution, %	Conformational distribution, %
$C_1(C_{ref})$	0	1	1	1	1	0	42.61	34.72
C_2	0.397	1.955	0.705	0.9988	1.378	0.173	21.23	25.17
C_3	0.559	2.571	0.821	0.9994	2.112	0.432	16.29	16.42
C_4	0.746	3.528	0.673	0.9989	2.373	0.491	11.69	14.61
C_5	0.965	5.098	0.748	0.9998	3.817	0.781	8.18	9.08

from the rotational point of view. On the other hand, the obtained results for the vibrational contribution to the partition functions of all five conformers imply that the geometry of C_2, C_3, C_4, and C_5 conformers (with correspondingly low vibrational equilibrium constants) are more open and less rigid than the most stable conformer (C_{ref}). This means that, however, C_2, C_3, C_4, and C_5 conformers have less electronic stability, they are all more favored by consideration of the vibrational degrees of freedom. On the other hand, a stringent comparison between the values of the electronic contribution to the conformational distributions and total conformational distribution percents (reported in Table 3) confirms that the inclusion of the rotational and vibrational degrees of freedom reduces the total conformational population difference between the conformers, but does not change the order of total conformational distribution percents.

In order to evaluate the temperature effect on the conformational distribution population, the conformational equilibrium constants and conformational distribution percents have been calculated at temperatures of 348.15 K, 398.15 K, and 498.15 K for all conformers. The obtained results have been reported in Table 4. As we expected, with rising temperature the less stable conformers are more populated and their conformational distribution percent values increase. In Fig. 5, we have demonstrated the variation of distribution percents for all conformers with increasing temperature.

CONCLUSIONS

The main purpose of this computational study was to probe the binding energy of VP and DCQ ligands coordinating with the lanthanide cation series ($Ln^{3+} = La^{3+}$, Ce^{3+}, Nd^{3+}, and Sm^{3+}). The evolution of metal—ligand bond distances with the lanthanide cation series was also discussed. According to our results, the increasing trend in the binding strength of ligands with the lanthanide cation series conforms first to the shortening of the Ln—N bond length and second to the diminution of the ionic

Table 4

Total conformational distribution percents of the $[Sm(VP)_2(DCQ)_3]^{3+}$ *complex at various temperatures*

Conformer	298.15 K	348.15 K	398.15 K	498.15 K
$C_1(C_{ref})$	34.695	31.414	29.039	25.858
C_2	25.170	25.177	25.076	24.785
C_3	16.425	17.063	17.483	18.255
C_4	14.618	15.918	16.896	17.977
C_5	9.089	10.425	11.504	13.122

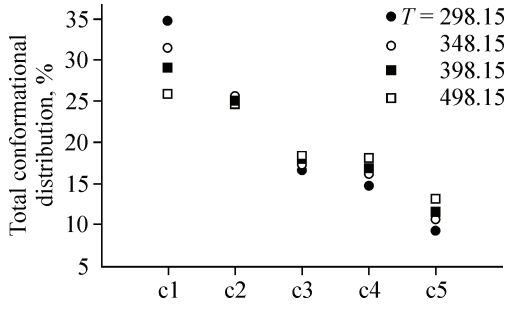

Fig. 5. Variation of the total conformational distribution percents for five conformers of the $[Sm(VP)_2(DCQ)_3]^{3+}$ complex at various temperatures

radius of lanthanide cations. These findings are consistent with the electrostatic nature of lanthanide—ligand interactions. Due to the ionic character of lanthanide—ligand bonds, we have considered the solvent effects through PCM calculations that presented a more precise description for the lanthanide—ligand interactions. Then, by calculating deformation energy values in the lanthanide cation series, it was deduced that the ligands are more deformed by harder metal cations. Finally, the analysis of conformational equilibrium constants for the $[Sm(VP)_2(DCQ)_3]^{3+}$ complex indicates that although the conformer (C_{ref}) should be favored with respect to all the other conformers from the electronic viewpoint, the inclusion of rotational and vibrational degrees of freedom reduces the conformational population difference between the conformers, while it does not affect remarkably the order of conformational distribution percents. We have also demonstrated that with rising temperature the less stable conformers are more populated and their conformational distribution percent values increase.

Acknowledgments. The first author gratefully acknowledges partial financial support from the research council of Alzahra University.

REFERENCES

1. *Daniel S.*, *Babu E.J., Prasada Rao T.* // Talanta. – 2005. – **65**. – P. 441 – 452.
2. *Metilda P.*, *Gladis J.M.*, *Venkateswaran G. et al.* // Anal. Chim. Acta. – 2007. – **587**. – P. 263 – 271.
3. *Metilda P.*, *Gladis J.M., Prasada Rao T.* // Anal. Chim. Acta. – 2004. – **512**. – P. 63 – 73.
4. *Shirvani-Arani S.*, *Ahmadi S.J.*, *Bahrami-Samani A. et al.* // Anal. Chim. Acta. – 2008. – **623**. – P. 82 – 88.
5. *Kala R.*, *Gladis J.M., Prasada Rao T.* // Anal. Chim. Acta. – 2004. – **518**. – P. 143 – 150.
6. *Biju V.M.*, *Gladis J.M., Prasada Rao T.* // Anal. Chim. Acta. – 2003. – **478**. – P. 43 – 51.
7. *Prasada Rao T.*, *Daniel S., Gladis J.M.* // Trends Anal. Chem. – 2004. – **23**. – P. 28 – 35.
8. *Prasada Rao T.*, *Kala R., Daniel S.* // Anal. Chim. Acta. – 2006. – **578**. – P. 105 – 116.
9. *Barone V., Cossi M.* // J. Phys. Chem. – 1998. – **A102**. – P. 1995 – 2001.
10. *Cosentino U.*, *Villa A., Pitea D.* // J. Phys. Chem. – 2000. – **B104**. – P. 8001 – 8007.
11. *Villa A.*, *Hess B., Saint-Martin H.* // J. Phys. Chem. – 2009. – **B113**. – P. 7270 – 7281.
12. *McQuarrie D.A.* Statistical Mechanics. – New York: Harper Collins, 1976.
13. *Becke A.D.* // J. Chem. Phys. – 1993. – **98**. – P. 1372 – 1377.
14. *Boehme C., Wipff G.* // Inorg. Chem. – 1999. – **38**. – P. 5734 – 5741.
15. *de Andrade A.V.M.*, *da Costa Jr N.B.*, *Simas A.M. et al.* // Chem. Phys. Lett. – 1994. – **227**. – P. 349 – 353.
16. *Freire R.O.*, *Rocha G.B., Simas A.M.* // Inorg. Chem. – 2005. – **44**. – P. 3299 – 3310.
17. *Freire R.O.*, *da Costa Jr N.B.*, *Rocha G.B. et al.* // J. Chem. Theory Comput. – 2006. – **2**. – P. 64 – 74.
18. *Freire R.O.*, *Mesquita M.E.*, *Couto dos Santos M.A. et al.* // Chem. Phys. Lett. – 2007. – **442**. – P. 488 – 491.
19. *da Costa Jr N.B.*, *Freire R.O.*, *Simas A.M. et al.* // J. Phys. Chem. – 2007. – **A111**. – P. 5015 – 5018.
20. *Cao X., Dolg M.* // Mol. Phys. – 2003. – **101**. – P. 2427 – 2435.
21. *Perrin L.*, *Maron L.*, *Eisenstein O. et al.* // Organometallics. – 2003. – **22**. – P. 5447 – 5453.
22. *Cosentino U.*, *Moro G.*, *Pitea D. et al.* // J. Phys. Chem. – 1998. – **A102**. – P. 4606 – 4614.
23. *Villa A.*, *Cosentino U., Pitea D.* // J. Phys. Chem. – 2000. – **A104**. – P. 3421 – 3429.
24. *Cosentino U.*, *Villa A.*, *Pitea D. et al.* // J. Amer. Chem. Soc. – 2002. – **124**. – P. 4901 – 4909.
25. *Cosentino U.*, *Pitea D.*, *Moro G. et al.* // Theor. Chem. Acc. – 2004. – **111**. – P. 204 – 209.
26. *Dolg M.*, *Stoll H., Preuss H.* // Theor. Chim. Acta. – 1993. – **85**. – P. 441 – 450.
27. *Dolg M.*, *Stoll H., Savin A. et al.* // Theor. Chim. Acta. – 1989. – **75**. – P. 173 – 194.
28. *Yang J., Dolg M.* // Theor. Chem. Acc. – 2005. – **113**. – P. 212 – 224.
29. *Weigand A.*, *Cao X.*, *Yang J. et al.* // Theor. Chem. Acc. – 2010. – **126**. – P. 117 – 127.
30. *Ditchfield R.*, *Hehre W.J., Pople J.A.* // J. Chem. Phys. – 1971. – **54**. – P. 724 – 730.
31. *Hehre W.J.*, *Ditchfield R., Pople J.A.* // J. Chem. Phys. – 1972. – **56**. – P. 2257 – 2268.
32. *Francl M.M.*, *Pietro W.J.*, *Hehre W.J. et al.* // J. Chem. Phys. – 1982. – **77**. – P. 3654 – 3662.
33. *Schmidt M.W.*, *Baldridge K.K.*, *Boatz J.A. et al.* // J. Comput. Chem. – 1993. – **14**. – P. 1347 – 1363.
34. MOPAC2009, James J.P. Stewart, Stewart Computational Chemistry, Version 8.331M, Colorado springs, USA, 2009.
35. *Shannon R.D.* // Acta Crystallogr. – 1976. – **A32**. – P. 751 – 767.
36. *David F.* // J. Less Common Met. – 1986. – **121**. – P. 27 – 42.
37. *David F.H., Fourest B.* // New J. Chem. – 1997. – **21**. – P. 167 – 172.
38. *Nash K.L.* // Solvent Extr. Ion Exch. – 1993. – **11**. – P. 729 – 768.
39. *Guillaumont D.* // J. Phys. Chem. – 2004. – **A108**. – P. 6893 – 6900.
40. *Chelli B.*, *Gervasio F.L.*, *Gellini C.*, *Procacci P.*, *Cardini G., Schettino V.* // J. Phys. Chem. – 2000. – **A104**. – P. 11220 – 11222.